

**184. Interconversion of (η^3 -Allyl)(η^4 -conjugated-diene)
(η^5 -cyclopentadienyl)zirconium and -hafnium Stereoisomers.
Evidence for the Simultaneous Rearrangement of Diene and Allyl Ligands**

by Christoph Sontag^a), Heinz Berke^a)*, Christian Sarter^b), and Gerhard Erker^b)*

^a) Anorganisch-chemisches Institut der Universität Zürich, Winterthurerstrasse 190, CH-8057 Zürich

^b) Institut für Organische Chemie der Universität Würzburg, Am Hubland, D-8700 Würzburg

(18. VIII. 89)

Reaction of (η^3 -allyl)(cyclopentadienyl)zirconium(4+) chloride with (2,3-dimethylbutadiene)magnesium or (2-phenylbutadiene)magnesium gave the (η^3 -allyl)(η^4 -conjugated diene)(cyclopentadienyl)zirconium complexes **3c** and **3d**, respectively. The analogous reaction between (η^3 -allyl)(cyclopentadienyl)hafnium(4+) chloride with (butadiene)magnesium afforded (η^3 -allyl)(η^4 -butadiene)(η^5 -cyclopentadienyl)hafnium **3e**. Photolysis of the complexes **3** produced their stereoisomers **4**. The open-chain π ligands in **3** open themselves towards the apical Cp ligand, in **4** they both are turned around by 180°. The *Gibbs* activation energy of the **4** \rightarrow **3** rearrangement of the Hf complex does not deviate significantly from those of the Zr-containing systems (**4c** \rightarrow **3c**: ΔG^\ddagger rearr. (-10°) = 81.1 ± 1.3 kJ/mol; **4d** \rightarrow **3d**: ΔG^\ddagger (-10°) = 85.7 ± 1.3 kJ/mol; **4e** \rightarrow **3e**: ΔG^\ddagger (-5°) = 84.4 ± 1.3 kJ/mol). A modified extended-*Hückel* theory (MEHT) was used in order to simulate the thermally induced rearrangement of the diene ligand in **3/4**. The calculations indicate that there should be a combinational interconversion of both the diene and allyl ligand. A diene inversion becomes energetically favoured, if a simultaneous allyl rotation occurs. The transition state **9** lies ca. 90 kJ/mol above the optimized geometry of **4a** and 115 kJ/mol above **3a**. Orbital considerations show that a spatially different 'valence' orbital of the [Zr(allyl)Cp] fragment **6** in comparison with [ZrCp₂] **7** causes the conformational preference of the diene ligand in **3a** with a higher rearrangement barrier.

Introduction. – Two (η^3 -allyl)(η^4 -butadiene)(η^5 -cyclopentadiene)Zr stereoisomers have been described in [1]. The reaction of (η^3 -allyl)(η^5 -cyclopentadiene)zirconium(4+) chloride (**1a**) with (butadiene)magnesium (**2a**) yields the complex **3a**, characterized by both the π -allyl and the *s-cis*- η^4 -butadiene ligand opening themselves towards the apical cyclopentadienyl group at the Zr-atom. Irradiation with UV light ($\lambda > 300$ nm) at low temperature rapidly produces the stereoisomeric (η^3 -allyl)(*s-cis*- η^4 -butadiene)(η^5 -cyclopentadiene)zirconium (**4a**) where both open-chain π ligands have their 'meso'-CH groups being directed towards the cyclopentadiene (Cp) ligand. Complex **4a** undergoes a clean thermally induced rearrangement to give **3a**. The isomerization reaction follows first-order kinetics with a *Gibbs* activation energy of ΔG^\ddagger ($+10^\circ$) = 92.4 ± 1.3 kJ/mol. The (η^3 -allyl)Cp(η^4 -isoprene)Zr system behaves analogously (**4b** \rightarrow **3b** rearrangement: ΔG^\ddagger (-10°) = 81.9 ± 1.3 kJ/mol).

There is evidence that [ZrCp]-bound allyl ligands can undergo rapid isomerization reactions [2]. For the rearrangement of the (diene)CpZr structural subunit, two principally different 'classical' reaction types can be visualized. The interconversion of the (η^3 -allyl)Cp(diene)Zr isomers could take place by means of a diene rotation (proceeding concerted or stepwise *via* (η^2 -diene)- or (η^3 -dienyl)metal complex intermediates) or a topomerization mechanism (*i.e.* a 'ring inversion' of the (*s-cis*-diene)M metallacyclic

framework). The former pathway is commonly observed for many (*s-cis*- η^4 -conjugated diene)metal complexes, especially of the late transition elements (for typical examples, see [3]). In contrast, the ‘ring-flip’ isomerization mechanism is typical for a variety of early transition metal diene complexes [4]. There is no easy *a priori* distinction between these alternatives for the 3 \rightleftharpoons 4 stereoisomerization. Therefore, we have analyzed the 3 \rightleftharpoons 4 interconversion using EHMO methods and compared the outcome of our model calculation with some results originating from an additional experimental study.

Experimental Studies. – The automerization of (*s-cis*- η^4 -conjugated diene)(group IV) metallocene complexes **5** takes place by a ‘ring-flip’ mechanism *via* a metallacyclopentene transition-state geometry [5][†]. The activation barrier of the 5 \rightleftharpoons 5' rearrangement is dominated by ground-state effects (*Scheme 1*). Increasing the metallacyclopentene character of the diene complexes **5** leads to decreasing $\Delta G^\ddagger_{\text{inv.}}$ values of the automerization

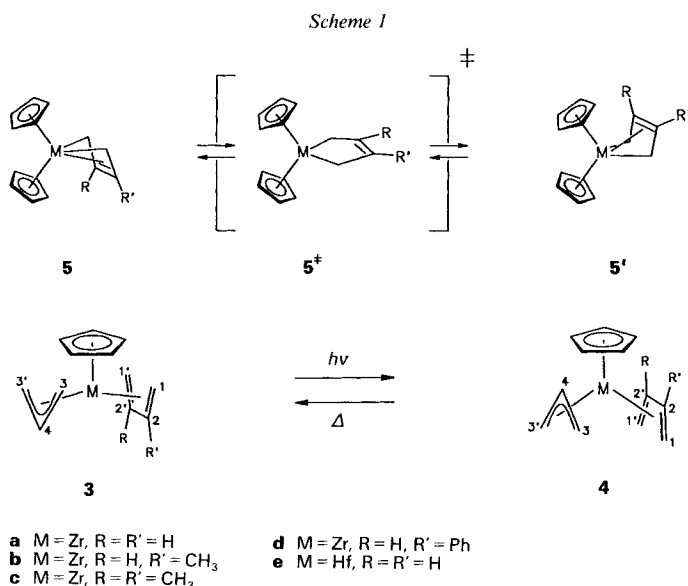


Table 1. A Comparison of Gibbs Activation Energies^{a)} of the 4 \rightarrow 3 Isomerization of [M(η^3 -Allyl)(η^4 -conjugated diene)Cp] Complexes and the Automerization of Related (*s-cis*- η^4 -diene)metallocenes **5**^{b)}

Diene ligand	Metal	(Allyl)Cp complex	$\Delta G^\ddagger_{\text{rearr.}}$ (T [°C])	Metallocene complex	$\Delta G^\ddagger_{\text{inv.}}$ (T [°C])
Butadiene	Zr	4a	92.4 (10)	5a	52.8 (-19.5)
Isoprene	Zr	4b	81.9 (-10)	5b	51.0 (-29)
2,3-Dimethylbutadiene	Zr	4c	81.1 (-10)	5c	48.1 (-42)
2-Phenylbutadiene	Zr	4d	85.7 (-10)	5d	50.2 (-30)
Butadiene	Hf	4e	84.4 (-5)	5e	33.9 (-108)

^{a)} $\Delta G^\ddagger \pm 1.3$ kJ/mol.

^{b)} $\Delta G^\ddagger_{\text{inv.}}$ Values of complexes **5** are from [4a] (**5a, b, c, e**) and [5] (**5d**). $\Delta G^\ddagger_{\text{rearr.}}$ Values for complexes **4a, b** are from [1b].

process [4a]. This can *e.g.* be effected by placing alkyl or aryl substituents at the diene positions C(2) and/or C(3) or by changing the metal from Zr to Hf. The latter is known to form somewhat stronger metal-to-carbon σ -bonds. Typical diene-substituent/central metal dependent *Gibbs* activation energies of the diene-metallocene topomerization reaction are given in *Table 1* for the complexes **5a–e**. For a mechanistic characterization of the **4**→**3** rearrangement, it appeared necessary to compare the corresponding ΔG^\ddagger values of equivalent pairs of conjugated diene complexes of the (η^3 -allyl)CpZr and Cp₂Zr moieties (**4/3 vs. 5**)¹.

The synthesis of the (allyl)(conjugated diene)(cyclopentadienyl)group-IV-metal complexes is straightforward as shown for the example of the Hf complex **3e**. Radical chain chlorination [7] of [Hf(Cp)₂]Cl₂ in CCl₄ afforded a mixture of [Hf(Cp)]Cl₃ and HfCl₄. Treatment of the 55:45 mixture of these two metal halides with allylmagnesium chloride at low temperature readily produced a mixture of the corresponding allyl transition-metal complexes. The desired product [Hf(allyl)₃(Cp)] was separated from the better soluble [Hf(allyl)₄] by crystallization and then comproportionated with 2 mol-equiv. of [Hf(Cp)]Cl₃ to give (allyl)(cyclopentadienyl)hafnium dichloride (**1b**). Its treatment with the (butadiene)magnesium reagent [8] gave (η^3 -allyl)(η^4 -butadiene)(η^5 -cyclopentadienyl)hafnium (**3e**).

Complex **3e** is readily characterized by its typical ¹H- and ¹³C-NMR spectra (see *Tables 2* and *3*). Photolysis at low temperature almost quantitatively transforms the Hf complex **3e** into its stereoisomer **4e**. The thermally labile photoisomer **4e** can readily be distinguished from the more stable **3e** by typical variations of its NMR parameters (*e.g.* pronounced upfield shift of the Cp ¹H/¹³C resonances: $\delta = 6.02/108.5$ for **3e**, $\delta = 4.49/99.0$ for **4e**; see also *Tables 2* and *3*) [1].

The Zr complexes **3/4c** and **d** were obtained analogously, *i.e.*, starting from [Zr(Cp)₂]Cl₂ via [Zr(Cp)]Cl₃ [7], [Zr(allyl)₃(Cp)] [3], and [Zr(allyl)(Cp)]Cl₂ (**1a**) [1]. Reaction of **1a** with (2,3-dimethylbutadiene)magnesium [9] gave **3c**. Treatment of **1a** with the new (2-phenylbutadiene)magnesium reagent afforded **3d**. Irradiation cleanly converted these [Zr(allyl)Cp(diene)] complexes to the photoisomers **4c** and **4d**.

Table 2. A Comparison of Selected ¹H-NMR Data of Complexes **3** and **4**^{a)}

	Cp	Diene			Allyl			CH ₃	Ph
		H _a -C(1)	H _γ -C(1)	H-C(2)	H _a -C(3)	H _γ -C(3)	H-C(4)		
3c	6.08	-0.64	1.68		1.43	1.68	5.50	1.76	–
4c	4.61	-1.62	3.39		1.22	3.18	6.11	1.91	–
3d	6.11	-0.71	2.46	5.98	2.01	1.23	5.47	–	7.11
		-0.24	2.21		1.50	1.12			
4d	4.45	-1.95	4.00	5.55	1.47	3.31	6.04	–	7.34
		-0.93	3.62		0.69	3.17			7.08
3e^{b)}	6.02	-1.07	1.88	5.33	1.28	1.64	6.09	–	–
4e^{b)}	4.49	-1.80	3.57	5.03	0.97	3.23	5.85	–	–

^{a)} (D₈)Toluene, *T* = 203 K (**4c**), 223 K (**4d**), 213 K (**4e**), 300 K (**3c–e**), chemical shifts rel. TMS, δ scale.

^{b)} Coupling constants [Hz]: **3e**: *J*(H, H) = 9.7 (1s, 2); 10.4 (1a, 2); 8.6 (2, 2'); -8.3 (1s, 1a); 1.9 (1s, 2'); -1.9 (1a, 2'); 1.0 (1s, 1a'); 9.2 (3s, 4); 14.5 (3a, 4); 1.5 (3s, 3a); **4e**: *J*(H, H) = 8.7 (3s, 4); 16.1 (3a, 6); 2.0 (3a, 3s). *a*: 'anti', *s*: 'syn', with respect to the *meso*-protons (diene, H-C(2); allyl, H-C(4)).

¹⁾ For additional rearrangement pathways of (η^4 -conjugated diene)Cp₂M systems (M = Zr, Hf), see [6].

Table 3. $^{13}\text{C-NMR}$ Data of Complexes **3** and **4**^{a)}

	Cp	Diene		Allyl		CH ₃	Ph
		C(1)	C(2)	C(3)	C(4)		
3c ^{b)}	108.7	52.2	118.2	59.1	127.3	22.4	–
4c ^{b)}	101.7	54.0	108.3	56.9	121.0	23.4	–
3d ^{b)}	109.1	48.2	122.5	60.6	124.6	–	142.4, 128.5
		48.0	110.5	59.1			
4d ^{b)}	101.8	55.2	114.4	57.4	119.1	–	144.6, 128.4
		48.6	97.0	56.0			
3e ^{b)}	108.5	43.3	112.3	54.6	126.3	–	–
4e ^{b)}	99.0	45.4	99.5	55.9	115.9	–	–

^{a)} (D₈)Toluene, $T = 203\text{ K}$ (**4c**), 223 K (**4d**), 223 K (**4e**), 303 K (**3c–e**), chemical shifts rel. TMS, δ scale.

^{b)} Coupling constants [Hz]: **3c**: $^1J(\text{C}, \text{H}) = 168$ (Cp), 146 (C(1)), 155 (C(3)), 152 (C(4)), 124 (CH₃). **4c**: $^1J(\text{C}, \text{H}) = 168$ (Cp), 145 (C(1)), 139 (C(3)), 145 (C(4)), 125 (CH₃). **3d**: $^1J(\text{C}, \text{H}) = 171$ (Cp), 158 (C(2')), 155, 156 (C(3), C(3')), 157 (C(4)). **4d**: $^1J(\text{C}, \text{H}) = 173$ (Cp), 148, 150 (C(1), C(1')), 153 (C(2')), 147, 160 (C(3), C(3')), 148 (C(4)), 153, 157, 158 (Ph). **3e**: $^1J(\text{C}, \text{H}) = 171$ (Cp), 146 (C(1)), 160 (C(2)), 152 (C(3)), 156 (C(4)). **4e**: $^1J(\text{C}, \text{H}) = 173$ (Cp), 148 (C(1)), 156 (C(2)), 148, 159 (C(3)), 148 (C(4)).

The thermally induced rearrangements of the complexes **4c–e** to the thermodynamically favoured isomers **3c–e** were kinetically followed at one temperature each by $^1\text{H-NMR}$ spectroscopy. The rearrangement of each of the complexes **4** follows first-order kinetics. *Gibbs* activation energies for the **4a–e** \rightarrow **3a–e** rearrangements ($\Delta G^\ddagger_{\text{rearr.}}$) are listed in *Table 1* together with corresponding $\Delta G^\ddagger_{\text{inv.}}$ values of the diene-metallocene topomerization ('ring-flip') of the corresponding (*s-cis*- η^4 -conjugated diene)(Cp)₂M complexes **5a–e**, for comparison.

It is noteworthy, that the ΔG^\ddagger values of the **4** \rightarrow **3** rearrangement of the [Zr(allyl)(Cp)(diene)] complexes deviate from one another only marginally (80–90 kJ/mol). Rearrangement (*i.e.* automerization) of the corresponding [Zr(Cp)₂(diene)] complexes is much faster. The $\Delta G^\ddagger_{\text{inv.}}$ values for the complexes **5a–d** are *ca.* 50 kJ/mol, again not deviating very much from each other. Very characteristically, though, upon changing the central metal-atom from Zr to Hf has severe consequences on the activation barrier of the ring-inversion mechanism observed with the (diene)metallocene complexes. The Hf(butadiene) moiety has a much higher σ complex character as compared to the Zr analogue, and hence the $\Delta G^\ddagger_{\text{inv.}}$ activation barrier is drastically reduced. This effect is not being observed in the [M(allyl)(Cp)(diene)] series. [Hf(η^3 -Allyl)(η^4 -butadiene)(Cp)] shows a ΔG^\ddagger value for the **4** \rightarrow **3** rearrangement that deviates not significantly from the activation energies for this process of the corresponding Zr complexes. In fact, the *Gibbs* activation energy for the **4e** \rightarrow **3e** rearrangement attains a good average position in the **4a–e** \rightarrow **3a–e** series. These results indicate non-identical mechanistic types being operative in the thermally induced rearrangements of [M(allyl)(Cp)(η^4 -diene)] and [M(Cp)₂(η^4 -diene)] complexes.

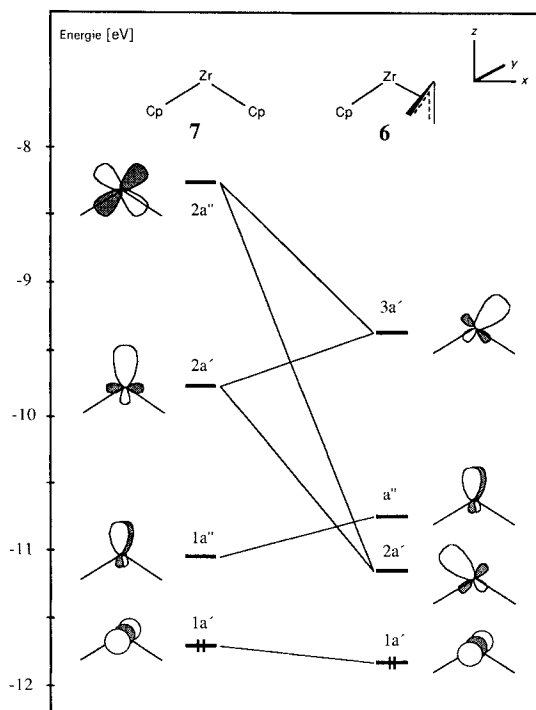
Calculations. – *Theoretical Analysis of a (Allyl)(butadiene)(cyclopentadiene)zirconium Complex.* MEHT calculations [10] on the **4a** \rightarrow **3a** process were carried out to find support for chemically plausible mechanisms of the **4** \rightarrow **3** rearrangement (for the EH parameters, see *Table 4*). It is appropriate to start this theoretical analysis with an evaluation of the orbital properties of **3a**. They can be best understood by composing

Table 4. *Extended Hückel Atomic Parameters Used in the MEHT Calculations*

Element	Orbital	H_{ii} [eV]	ζ_1	ζ_2	C_1	C_2	Ref.
H	1s	-13.6	1.30				[17]
L	1s	-11.4	1.20				
C	2s	-21.4	1.625				[17]
	2p	-11.4	1.625				
O	2s	-32.3	2.275				[17]
	2p	-14.8	2.275				
Zr	4d	-12.1	3.835	1.505	0.6211	0.5796	[16]
	5s	-10.1	1.776				
	5p	-6.86	1.817				

them from the interaction of the functions of a $[\text{Zr}(\text{allyl})(\text{Cp})]$ fragment **6** and a butadiene molecule. The valence orbitals of **6** are related to the well-known ones of a $[\text{Zr}(\text{Cp})_2]$ fragment **7** [11] and are qualitatively similar to the picture obtained by the analysis of $[\text{Ta}(\text{Cp})]\text{Cl}_2$ and $[\text{Zr}(\text{NH}_3)\text{Cp}]\text{Cl}$ moieties [12]. *Fig. 1* shows a correlation of the frontier orbital energy levels of $[\text{Zr}(\text{Cp})_2]$ and $[\text{Zr}(\text{allyl})(\text{Cp})]$ fragments.

In *Fig. 1*, the a'' and $1a'$ 'valence' orbitals (orbital notations with respect to C_s symmetry) of **6** and **7** are quite comparable in their shapes and energies. The formal replacement of a Cp by an allyl ligand which has a reduced bonding capability in the xz plane allows metal- d_{xz} character to be mixed into the $2a'$ and $3a'$ orbitals of **6**. Two d_{xz} -like



*Fig. 1. A correlation of the valence orbitals of a $[\text{ZrCp}_2]$ (**7**) and a $[\text{Zr}(\text{allyl})\text{Cp}]$ (**6**) fragment*

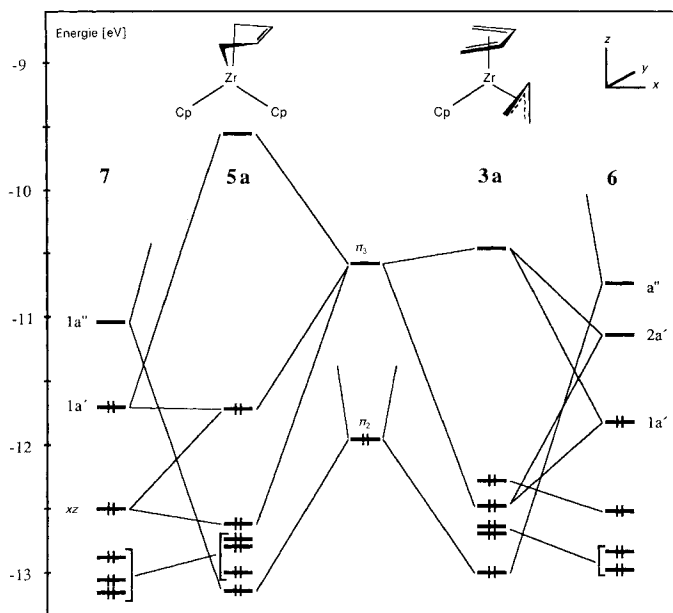


Fig. 2. MO-Interaction scheme of butadiene and $[ZrCp_2]$ (**7**) and $[Zr(allyl)Cp]$ (**6**) fragment orbitals

MO's with left/right asymmetry are formed, one of which is strongly directed toward the Cp ($2a'$) and the other one toward the allyl ligand ($3a'$).

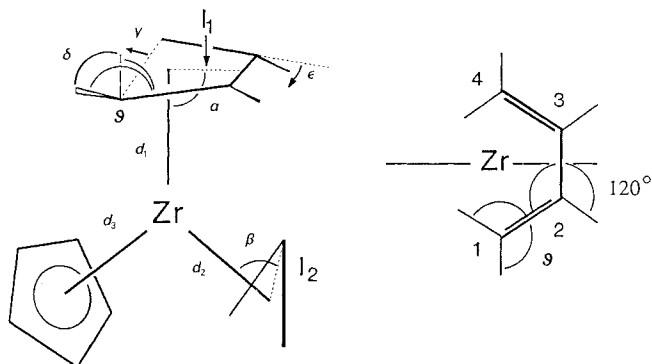
The $3a'$ orbital is relatively high-lying in energy because of an out-of-phase situation between metal-d and Cp orbital character and should, therefore, normally not be involved in valence interactions. The energetically lower $2a'$ MO, on the other hand, reflects only very little repulsion between metal-d and allyl character. This low-lying $2a'$ MO allows additional valency in the xz plane which was not available in **7**.

Starting from the 'valence' orbitals of **7** and **6** (Fig. 1) the bonding features of a butadiene can be seen from a MO-interaction scheme (Fig. 2). The geometries of the diene complexes were optimized with respect to their essential degrees of freedom (see Tables 5 and 6).

The two main interactions between the butadiene ligand and the metal fragments consist in both cases of diene-donor ($\pi_2 - a''$) and -acceptor ($\pi_3^* - 1a'$) interactions. The backbonding between metal fragment orbitals and the diene-LUMO (π_3^*) shows an essential difference between **3a** and **5a**. In the case of **5a**, we find a three-orbital interaction between metal $1a'$, a mainly ligand-oriented d_{xz} -character orbital and the π_3^* MO

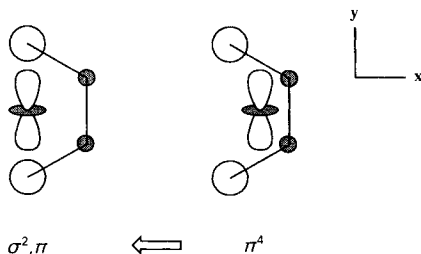
Table 5. Fixed Geometry Parameters (Idealized) of the $[Zr(allyl)(butadiene)Cp]$ and $[Zr(butadiene)Cp_2]$ Model Complexes Used during Geometry-Optimization Procedures

Cp ligand		Allyl ligand		Butadiene ligand	
C–C distance	135.8 pm	C–C distance	144 pm	C–H distance	103 pm
C–H distance	100.4 pm	C–H distance	103 pm	C–C–C angle	120°
Cp–Zr–Cp angle in 5a	120°	C–C–C angle	120°	C–C–H angle	120°
Cp–Zr–allyl angle in 3a	120°	C–C–H angle	120°		

Table 6. *Optimized Geometry Parameters for the [Zr(allyl)(butadiene)Cp] and [Zr(butadiene)Cp₂] Model Complexes Following the Notations of the Sketches Shown Below*

Distance Zr–diene	d_1	155.8	176.6 pm	Diene C–C distance		
Shift of diene	l_1	141.3	134.0 pm	C(1)(3)–C(2)(4)	158.6	159.8 pm
Bending angle	α	98.4	116.8°	C(2)–C(3)	151.6	15.2 pm
C–H bending	γ	40.0	49.3°	Distance Zr–allyl	d_2	215.1 – pm
	δ	144.6	139.9°	Distance Zr–Cp	d_3	192.8 198.8 pm
	ε	9.8	13.2°	Shift of allyl	l_2	32.0 – pm
C–H bond angle	ϑ	115.7	113.9°	Bending angle	β	103.9 – pm

leading to a nonbonding situation in the relatively high-lying HOMO. The stabilizing influence of the $1a'$ metal orbital on this MO depends on the diene shift with respect to the metal–diene bond axes. In an optimized σ^2, π position with a large diene shift, there is a good overlap between the $1a'$ and the terminal diene p_z functions (see Fig. 3). An artificial extreme π^4 binding of the diene unit, close to the situation in **3a**, would cause in **5a** the $1a'$ MO shifted into the nodal plane of the π_3^* diene MO.

Fig. 3. *Dominating orbital contributions to the HOMO in 5a*

Since the orbital combination in Fig. 3 represents the stabilizing contribution, the energy of the HOMO would be raised in case of π^4 bonding and, thus, forces the molecule to relax its diene unit toward a σ^2, π binding situation.

In a 14-electron species like **3a**, there are two electrons less. The corresponding high-lying MO represents now the LUMO which has naturally no influence on the structure of **3a**.

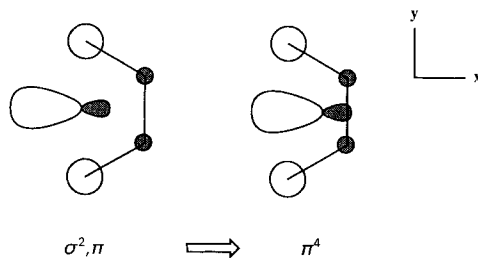


Fig. 4. Dominating orbital contributions to the back bonding interaction between butadiene and $[Zr(allyl)Cp]$ fragment orbitals

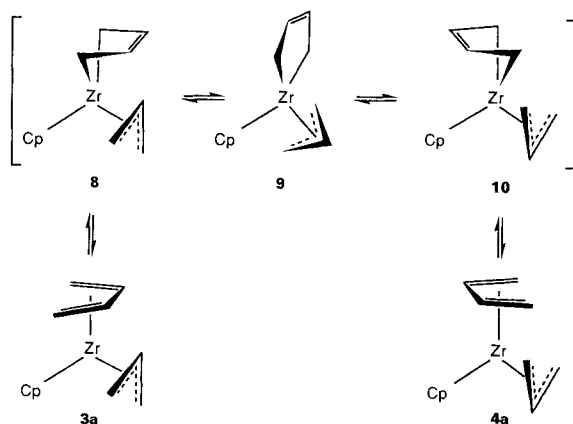
A more pronounced π^4 binding of the diene ligand in **3a** is supported by an additional effect. In this geometry, there is a participation of the $2a'$ metal fragment orbital character in the $1a' - \pi_3^*$ function utilizing the additional overlap capabilities of this directed d_{xz} -like orbital (Fig. 4).

Generally, such an orbital situation should disfavor a diene inversion process in the complexes **3**. In accord with this conclusion, we found a significant difference in the total overlap population between fragment orbitals of **6** and **7** and butadiene orbitals: the ratio is *ca.* 1.0:0.7 indicating an enhanced Zr–diene bond strength in **6** and hence smaller mobility of the diene ligand.

The intervention of the left/right asymmetric $2a'$ fragment orbital in **3a** also explains the found conformational preference of the diene ligand with its terminal C-atoms directed toward the Cp moiety. In this position, overlap between the emphasized p_z functions at the terminal C-atoms in the π_3^* diene and the $2a'$ fragment orbital is maximized.

Analysis of the Dynamic Features of the $[Zr(allyl)(butadiene)Cp]$ Model Compound. The activation barrier of the thermally induced reaction of **4** \rightarrow **3** (Scheme 1) was found to be in the order of 90 kJ/mol (see Table 3). The simulation of this thermal process by a

Scheme 2. Proposed Pathway for the Rearrangement of the Diene and Allyl Ligand from **3a** to **4a**



MEHT analysis revealed a combination of allyl- and diene-ligand motion to be the favoured mechanistic pathway (*Scheme 2*).

Modelling of chemical reactivity by quantum-chemical methods always involves a simplified view when interpreting the data in terms of thermodynamic parameters. Having this in mind, we nevertheless dare a mapping of our theoretical results on the elementary step $4 \rightarrow 3$, because we find an extremely good agreement with the experimental values.

The combination of diene inversion and allyl rotation gives rise to a transition state **9** with an electronic energy of *ca.* 90 kJ/mol above the conformer **4a** as established by a computed potential-energy surface. There are two important reaction coordinates for the model process $8 \rightarrow 10$: the bending angle α of a σ^2, π -bonded diene ligand and the rotational angle ω of the allyl moiety. In the ground state conformation **8**, these values are optimized to be 104° and 0° , respectively. These two angles were varied in steps of 10° , and in each combination, the other geometrical parameters were optimized to yield a minimum of total energy. In Fig. 5 this energy is plotted *vs.* the two variable angles and is scaled to the total electronic energy of the fully optimized structure of **3a** (see *Table 6*).

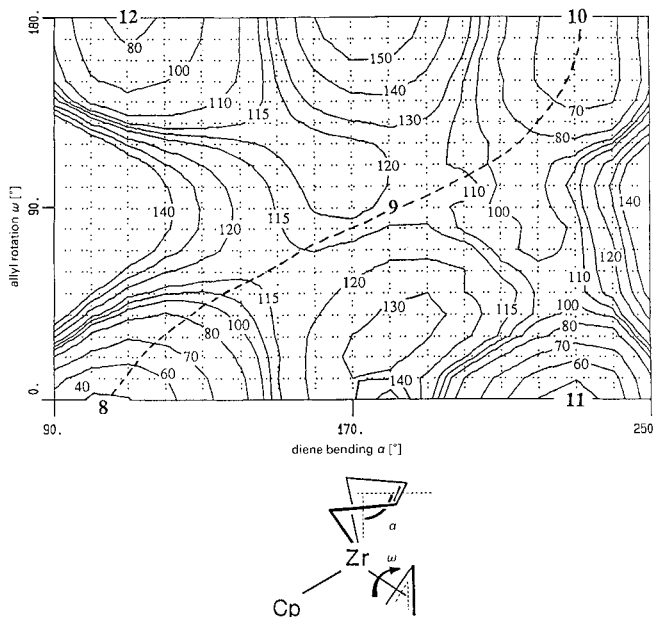
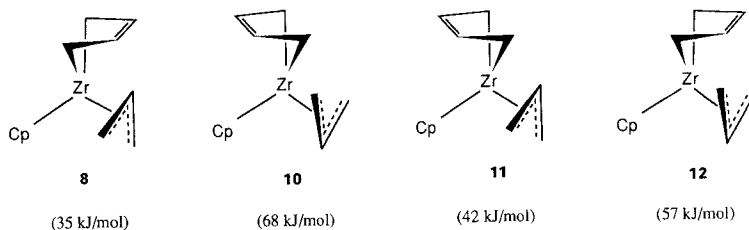


Fig. 5. Energy contour plot of the optimized geometries of the simultaneous allyl rotation and diene inversion $8 \leftrightarrow 10$ (energies in kJ/mol with respect to the fully optimized structure **3a**)

It is seen from this picture that there are four minima on the energy surface (in kJ/mol with respect to the fully optimized structure **3a**) corresponding to the possible combinations of the diene- and allyl-ligand positions (*cf.* **8–12**). Since these structures contain an artificially bound σ^2, π butadiene unit in order to allow a diene-inversion process, their energies reflect only thermodynamic trends of possible intermediate isomers.



All of these minima are connected by a saddle point representing the transition state **9**. From *Fig. 5*, it becomes obvious that a sole re-orientation of either of the ligands along one of the angle axes would cause an unfavourable activation barrier of *ca.* 150 kJ/mol.

The potential energy surface (*Fig. 5*) suggests that the photochemically produced isomer **10** should be energetically in close vicinity to the thermodynamic levels of the conformations **11** and **12**. The transition state **9** can be reached by a thermal process starting from these structures; **8** would then operate as an energetic sink on all motions on the potential-energy surface.

The photochemical reaction **3a** → **4a** can unfortunately not be analyzed, since there are fundamental difficulties to treat the photochemically induced open-shell systems within the extended *Hückel* formalism. For the thermal process **4a** → **3a**, potential-energy surfaces for alternative pathways were computed: a σ^2, π diene inversion like in **5**, and η^4 -diene rotation found for later transition-metal compounds, and a rotation of an η^3 - and η^2 -bound diene, in each case followed by an allyl-ligand rotation. The ¹H-NMR spectra of **3a** revealed a η^3 - η^1 dynamic allyl-ligand process with an activation barrier of *ca.* 80 kJ/mol [1b]. In our calculations, we were able to model the transition state for such a rearrangement of **3a**, finding an activation barrier of 106 kJ/mol. In addition, we computed η^1 -allyl geometries in combination with any of the aforementioned diene transition-state conformations. Even though extensive energetic optimization efforts on these pathways were carried out, we found for all processes significantly higher activation barriers of > 150 kJ/mol.

The Transition State 9. The result of the energy-surface analysis indicates that there must be a stabilizing effect on the diene inversion arising from the simultaneous allyl rotation. To reduce the [Zr(allyl)(butadiene)Cp] system to a simplified model, we considered the orbital situation in a d^0 -[ZrCpL₄]⁻ compound **13** replacing the noncyclic C ligands by pseudoligands L bearing a singly occupied 1s orbital (*Scheme 3*).

To describe the geometry of **13a** as a model for **9**, we compared it with the alternative structure **13b** which would represent a model for a transition state **14** of a sole diene

Scheme 3. Derivation of the Two Model Compounds [ZrCpL₄]⁻ from Two Transition-State Geometries **9** and **14**



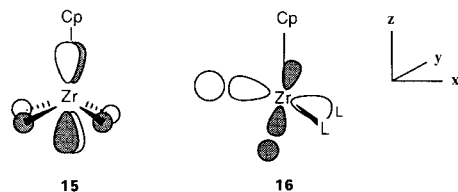


Fig. 6. Orbital representations of the decisive functions in **13a** and **13b**

inversion process. Fragmental orbital analysis composed of a $[\text{ZrCpL}_2]^+ + 2 \text{L}$ units in a pyramidal conformation **13b** shows that, for geometrical and therefore overlap reasons, the out-of-phase combination of the L_2 orbitals can only match with d_{yz} σ -type functions of the $[\text{ZrCpL}_2]^+$ fragment. This situation leads to a relatively high-lying, nearly nonbonding HOMO **15** with predominantly d_{yz} metal character.

In **13a**, we find a much more economic energetic situation which is caused by an effective exploitation of empty fragmental orbital character. The dominating stabilizing interaction consists of the out-of-phase combination of the L_2 unit with the well known $2a'$ $[\text{MCpL}_2]$ fragment MO which is unoccupied in the d^0 case [13]. This leads to a low-lying MO **16**.

In another approach similar to the analysis of *Hoffmann et al.* [14], we constructed a seven-coordinate model compound for the transition state **9**: the $\text{M}-\text{Cp}$ fragment can be replaced by a $[\text{ML}_3]$ system [15] and the other ligands by two donor ligands as in **13a** and **13b**, respectively (*Fig. 7*).

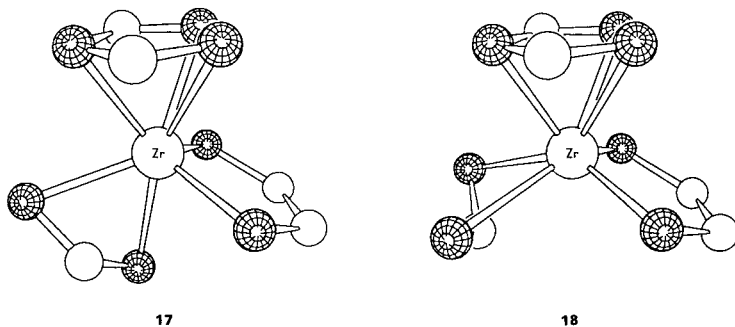


Fig. 7. Simplified representation of **9** and **14** as $[\text{ML}_7]$ species

The geometry of **9** resembles a 'capped trigonal-prismatic' polyhedron **17**. An alternative seven-coordinate 'trigonal base-tetragonal base' polyhedron **18** consisting of a three- and four-fold plane would be attributed to a transition-state geometry close to that of a solely butadiene inversion process. *Hoffmann et al.* showed that for d^0 complexes the geometry of a 'capped trigonal prism' should be favoured by *ca.* 45 kJ/mol in agreement with our analysis.

The MEHT calculations (*Table 4*) lead to the conclusion that rearrangement of both acyclic ligands in **3** should follow a mechanistic pathway with simultaneous inversion of

the diene and rotation of the allyl ligand. Orbital considerations show that the so-formed transition-state molecule **9** is favoured over such processes in which ligands are successively rearranged. This supports the indication from experimental work that, in the case of the complexes **3**, an unusual 'synergetic' effect between the rearrangement pathways of two apparently independent olefinic ligands take place.

We thank PD Dr. R. Benn, Dr. R. Mynott, and their coworkers at the Max-Planck-Institut für Kohlenforschung in Mülheim a.d. Ruhr for several NMR spectra. Financial support from the *Fonds der Chemischen Industrie*, the *Bundesminister für Forschung und Technologie*, and the *Alfried Krupp von Bohlen und Halbach-Stiftung* (grants to G. E.) is gratefully acknowledged.

Experimental Part

General. All reactions were carried out under Ar using *Schlenk*-type glassware. Solvents were dried (benzophenone/K or P₄O₁₀) and distilled under Ar prior to use. Deuterated solvents were dried with Na/K alloy ((D₈)toluene, (D₆)benzene) or P₄O₁₀ (CDCl₃, CD₂Cl₂) and distilled. Elemental analyses were carried out by *Dornis and Kolbe*, Mikroanalytisches Laboratorium, Mülheim a. d. Ruhr or the Institut für Anorganische Chemie der Universität Würzburg. M.p. (uncorrected) of the organometallic compounds were measured in sealed capillaries under Ar. NMR spectrometers used: *Bruker WP 200 SY, WH 400 FT*. EI-MS (70 eV). *Varian MAT CH5* mass spectrometer. The organometallic compounds [Zr(allyl)(cyclopentadienyl)]Cl₂ [**1b**], (butadiene)magnesium [**8**], and (2,3-dimethylbutadiene)magnesium [**9**] were prepared according to literature procedures.

(η^3 -Allyl)(η^4 -2,3-dimethylbutadiene)(η^5 -cyclopentadienyl)zirconium (**3c**). (2,3-Dimethylbutadiene)magnesium (2.02 g, 8.06 mmol), suspended in 30 ml of Et₂O, is added to a suspension of 2.16 g (8.05 mmol) of (allyl)(η -cyclopentadienyl)zirconium dichloride in 100 ml of Et₂O at -40° and stirred for 90 min. During this time the colour of the mixture changes from yellow to dark red. Solvent is removed at -40° *i.v.* The dark red residue is then extracted with 180 ml of pentane for 2 h at amb. temp. The dark red pentane soln. is cooled to -80° after filtration. Complex **3c** is obtained as a microcrystalline, purple solid: 1.02 g (45%). M.p. 185° (dec.). Anal. calc. for C₁₄H₂₀Zr (279.53): C 60.16, H 7.21; found: C 60.66, H 7.31.

(2-Phenylbut-2-ene-1,4-diyl)magnesium-bis(tetrahydrofuran) ('(2-phenylbutadiene)magnesium'). A soln. of 1.90 g of 2-phenylbutadiene (14.6 mmol) in 50 ml of THF is added with stirring to 5 g of activated Mg in 80 ml of THF. The mixture is stirred for five days at 15°. The resulting green brown suspension is filtered and the filtrate stripped *i.v.* The product is obtained as very air- and moisture-sensitive orange-red powder: 2.67 g (61%). M.p. 135°. Anal. calc. for C₁₈H₂₆MgO₂ (298.71): C 72.38, H 8.77; found: C 72.25, H 8.32.

(η^3 -Allyl)(η^4 -2-phenylbutadiene)(η^5 -cyclopentadienyl)zirconium (**3d**). To a suspension of 1.70 g of [Zr(allyl)Cp]Cl₂ (6.34 mmol) in 100 ml of Et₂O is added at -40° a suspension of 1.90 g of '(2-phenylbutadiene)magnesium' (6.36 mmol) in 30 ml of Et₂O. The mixture is stirred for 2 h at -40°. During this time it turns purple. Solvent is then removed *i.v.* at -30°. The residue is extracted with toluene at -10° and filtered. The product crystallizes at -80° from the toluene soln. Further material is obtained from the concentrated mother liquor at low temp.: 1.32 g (64%). M.p. 108° (dec.). Correct elemental anal. of the very pyrophoric compound could not be obtained. MS: 326 (M⁺), 285 (M⁺ - allyl), 283, 196 (M⁺ - 2-phenylbutadiene), 194.

(η -Cyclopentadienyl)hafnium Trichloride. A 500-ml two-necked *Schlenk* tube is charged with 10.2 g of finely powdered [HfCp₂]Cl₂ (26.8 mmol) and 300 ml of dry CCl₄ under Ar. Cl₂ (dried over H₂SO₄) is introduced slowly through a gas inlet tube ending shortly above the surface of the rapidly stirred suspension. A temp. increase indicates the beginning of the reaction. The temp. of the mixture is kept between 20 and 23° by adjusting the Cl₂ stream and occasional external cooling using an ice/water bath. The reaction is complete within *ca.* 30 min. Excess Cl₂ is removed from the mixture with Ar. The product is recovered by filtration and washed successively with 100 ml of CCl₄, 50 ml of CHCl₃, and 100 ml petroleum ether to give 8.7 g of a greyish coloured powder. According to the elemental anal. (calc. for [HfCp]Cl₃ (349.94): C 17.16, H 1.44, Cl 30.39; found: C 9.55, H 0.80, Cl 36.48), it contains *ca.* 55% [HfCp]Cl₃ besides HfCl₄. ¹H-NMR (CDCl₃, THF adduct): 6.41 (s, 5 H, Cp). The [HfCp]Cl₃/HfCl₄ mixture is used without further purification for the reaction with allylmagnesium chloride.

Tris(allyl)(η-cyclopentadienyl)hafnium. In a 300-ml Schlenk flask, 3.27 g of the [HfCp]Cl₃/HfCl₄ mixture (1.83 g CpHfCl₃, 5.23 mmol) are suspended in 100 ml of Et₂O at -78°. During 1 h, 80 ml of a 0.38M soln. of allylmagnesium chloride (30.4 mmol) are added dropwise. The resulting yellow mixture is stirred for 90 min at -25°. Solvent is removed at -25° *i.v.* The residue is stirred with pentane (200 ml) at -35° overnight. The mixture is filtered at -35° and the filtrate cooled to -80°. The product crystallizes to give an orange-red microcrystalline solid: 1.20 g (62%). The also formed tetraallylhafnium can be isolated from the concentrated mother liquor by crystallization. [Hf(allyl)₃Cp] is very thermolabile and should always be kept below -15°. ¹H-NMR ((D₈)toluene, -40°): 5.38 (s, 5 H, Cp); 5.48 (m, 3 H); 2.68 (d, 12 H, allyl-dynamic). ¹³C-NMR ((D₈)toluene, -40°): 108.8 (d, Cp, J(C, H) = 176); 137.9 (d, J(C, H) = 151); 75.7 (t, J(C, H) = 148, allyl-C).

(Allyl)(η-cyclopentadienyl)hafnium Dichloride (1b). A sample of 1.20 g of [Hf(allyl)₃Cp] (3.27 mmol) is dissolved at -40° in 100 ml of Et₂O. The soln. is given to 4 g of the [HfCp]Cl₃/HfCl₄ mixture (2.24 g [HfCp]Cl₃, 6.57 mmol) and stirred for 72 h at -40°. The resulting yellow suspension containing ca. 3.5 g [Hf(allyl)Cp]Cl₂ (ca. 9.8 mmol) is used without characterization for the following reactions. The suspension is stored at temp. below -10° to avoid decomposition.

(η³-Allyl)(η⁴-butadiene)(η-cyclopentadienyl)hafnium (3e). To a suspension of ca. 3.5 g of [Hf(allyl)Cp]Cl₂ (ca. 9.8 mmol), prepared as described above, in 100 ml of Et₂O is added at -40° a suspension of 2.30 g 'butadienemagnesium' (10.3 mmol) in 20 ml of Et₂O. The orange mixture is stirred for 90 min at -40°. Solvent is then removed at -40° *i.v.* The residue is stirred at ambient temp. with 150 ml of pentane for 1 h and then filtered. The product crystallizes from the filtrate upon cooling to -80° to give 1.22 g (37%). M.p. 196° (dec.). Anal. calc. for C₁₂H₁₆Hf (338.75): C 42.55, H 4.76; found: C 42.22, H 4.95.

Photoisomerization of the (η³-Allyl)(η⁴-conjugated diene)(η⁵-cyclopentadienyl)metal Complexes (3 → 4). The isomeric [M(allyl)Cp(diene)] complexes **4** were prepared by irradiation of solns. of the complexes **3** (samples of ca. 50 mg each in ca. 0.6 ml of (D₈)toluene) in sealed 5-mm NMR tubes (*Philips HPK 125*) at -60°. Complexes **4** were not isolated but identified by their very characteristic NMR spectra (see *Tables 2 and 3*) and the thermally induced rearrangement to the respective starting materials **3**.

Determination of the Gibbs Activation Energies of the Thermally Induced Rearrangement of the (η³-Allyl)(η⁴-conjugated diene)(η⁵-cyclopentadienyl)metal Complexes (4 → 3). The kinetics of the isomerization were determined by following the time-dependent concentration variations of complexes **4** and **3** by ¹H-NMR spectroscopy. The concentrations of the isomers were determined by integration of their respective cyclopentadienyl resonances. The **4** → **3** rearrangements all follow first-order rate laws with the following rate constants: **4c** → **3c**: $k = 4.00 \pm 0.04 \cdot 10^{-4} \text{ s}^{-1}$ at -10°; **4d** → **3d**: $k = 4.95 \pm 0.03 \cdot 10^{-5} \text{ s}^{-1}$ at -10°; **4e** → **3e**: $k = 2.10 \pm 0.04 \cdot 10^{-4} \text{ s}^{-1}$ at -5°.

REFERENCES

- [1] a) G. Erker, K. Berg, C. Krüger, G. Müller, K. Angermund, R. Benn, G. Schroth, *Angew. Chem.* **1984**, *96*, 445; b) G. Erker, K. Berg, R. Benn, G. Schroth, *Chem. Ber.* **1985**, *118*, 1383; c) G. Erker, K. Berg, R. Benn, G. Schroth, *Angew. Chem.* **1984**, *96*, 621; d) K. Berg, G. Erker, *J. Organomet. Chem.* **1984**, *270*, C53.
- [2] G. Erker, K. Berg, K. Angermund, C. Krüger, *Organometallics* **1987**, *6*, 2620.
- [3] L. Kruczynski, J. Takats, *J. Am. Chem. Soc.* **1974**, *96*, 932; *Inorg. Chem.* **1976**, *15*, 3140; C. G. Kreiter, S. Stüber, L. Wackerle, *J. Organomet. Chem.* **1974**, *66*, C49; M. A. Busch, R. J. Clark, *Inorg. Chem.* **1975**, *14*, 226; S. D. Ittel, F. A. Van-Catledge, J. P. Jesson, *J. Am. Chem. Soc.* **1979**, *101*, 3874; *J. Organomet. Chem.* **1979**, *168*, C25; M. Kotzian, C. G. Kreiter, S. Özkar, *ibid.* **1982**, *229*, 29; S. Özkar, C. G. Kreiter, *ibid.* **1986**, *303*, 367.
- [4] a) G. Erker, K. Engel, C. Krüger, A.-P. Chiang, *Chem. Ber.* **1982**, *115*, 3311; G. Erker, K. Engel, C. Krüger, G. Müller, *Organometallics* **1984**, *3*, 128; G. Erker, C. Krüger, G. Müller, *Adv. Organomet. Chem.* **1985**, *24*, 1; C. Krüger, G. Müller, G. Erker, U. Dorf, K. Engel, *Organometallics* **1985**, *3*, 215; G. Erker, K. Engel, C. Krüger, Y.-H. Tsay, E. Samuel, P. Vogel, *Z. Naturforsch., B* **1985**, *40*, 150; G. Erker, T. Mühlenbernd, R. Benn, A. Rufinska, Y.-H. Tsay, C. Krüger, *Angew. Chem.* **1985**, *97*, 336; G. Erker, T. Mühlenbernd, A. Rufinska, R. Benn, *Chem. Ber.* **1987**, *120*, 507; R. Benn, H. Grondey, R. Nolte, G. Erker, *Organometallics* **1988**, *7*, 777; see also: H.-B. Bürgi, K. C. Dubler-Stuedle, *J. Am. Chem. Soc.* **1988**, *110*, 4953; b) H. Yasuda, K. Tatsumi, A. Nakamura, *Acc. Chem. Res.* **1985**, *18*, 120; H. Yasuda, A. Nakamura, *Angew. Chem.* **1987**, *99*,

- 745; c) G. Erker, T. Mühlenbernd, R. Benn, A. Rufinska, *Organometallics* **1986**, *5*, 402; G.M. Smith, H. Suzuki, D.C. Sonnenberger, V.W. Day, T.J. Marks, *ibid.* **1986**, *5*, 549; d) J.W. Faller, A.M. Rosan, *J. Am. Chem. Soc.* **1977**, *99*, 4858; M. Bottrill, M. Green, *J. Chem. Soc., Dalton Trans.* **1977**, 2365; G. Wilke, *Fundam. Res. Homogeneous Catal.* **1979**, *3*, 1; R. Benn, G. Schroth, *J. Organomet. Chem.* **1981**, 228, 71; W.H. Hersh, F.J. Hollander, R.G. Bergman, *J. Am. Chem. Soc.* **1983**, *105*, 5834; B. Eaton, J.A. King, Jr., K.P.C. Vollhardt, *ibid.* **1986**, *108*, 1359.
- [5] G. Erker, U. Korek, unpublished.
- [6] a) G. Erker, K. Engel, U. Korek, P. Czisch, H. Berke, P. Caubere, P. Vanderesse, *Organometallics* **1985**, *4*, 1531; b) G. Erker, J. Wicher, K. Engel, F. Rosenfeldt, W. Dietrich, C. Krüger, *J. Am. Chem. Soc.* **1980**, *102*, 6344; G. Erker, J. Wicher, K. Engel, C. Krüger, *Chem. Ber.* **1982**, *115*, 3300; U. Dorf, K. Engel, G. Erker, *Organometallics* **1983**, *2*, 462; c) G. Erker, K. Engel, P. Vogel, *Angew. Chem.* **1982**, *94*, 791.
- [7] G. Erker, K. Berg, L. Treschanke, K. Engel, *Inorg. Chem.* **1982**, *21*, 1277.
- [8] K. Fujita, Y. Ohnuma, H. Yasuda, H. Tani, *J. Organomet. Chem.* **1976**, *113*, 201.
- [9] H. Yasuda, Y. Kajihara, K. Mashima, K. Nagasuna, K. Lee, A. Nakamura, *Organometallics* **1982**, *1*, 388.
- [10] A.B. Anderson, *J. Chem. Phys.* **1975**, *62*, 1187; D.A. Pensak, R.J. McKinney, *Inorg. Chem.* **1979**, *18*, 3407, 3413.
- [11] J.W. Lauher, R. Hoffmann, *J. Am. Chem. Soc.* **1976**, *98*, 1729.
- [12] H. Yasuda, K. Tatsumi, T. Okamoto, K. Mashima, K. Lee, A. Nakamura, Y. Kai, N. Kanehisa, N. Kasai, *J. Am. Chem. Soc.* **1985**, *107*, 2410; J. Blenkins, B. Hessen, F. van Bolhuis, A.J. Wagner, J.H. Teuben, *Organometallics* **1987**, *6*, 459.
- [13] B.E.R. Schilling, R. Hoffmann, D.L. Lichtenberger, *J. Am. Chem. Soc.* **1979**, *101*, 585.
- [14] R. Hoffmann, B.F. Beier, E.L. Muetterties, A.R. Rossi, *Inorg. Chem.* **1977**, *16*, 511.
- [15] T.A. Albright, *Tetrahedron* **1982**, *38*, 1339.
- [16] J. Howell, A. Rossi, D. Wallace, K. Haraki, R. Hoffmann, FORTICON8, QCPE Program No. 344, Indiana University, Bloomington.
- [17] K. Tatsumi, H. Yasuda, A. Nakamura, *Isr. J. Chem.* **1983**, *23*, 145.